ELSEVIER

Nuclear Instruments and Methods in Physics Research B 136–138 (1998) 654–660

NIM B
Beam Interactions with Materials & Atoms

Quantitative compositional depth profiling of $Si_{1-x-y}Ge_xC_y$ thin films by simultaneous elastic recoil detection and Rutherford backscattering spectrometry

S.C. Gujrathi [a,*], S. Roorda [a], J.G. D'Arcy [b], Randall J. Pflueger [b], P. Desjardins [b], I. Petrov [b], J.E. Greene [b]

[a] *Department of Physics and Groupe de recherche en physique et technologie des Couches Minces, Université de Montréal, P.O. Box 6128, Station Centre-Ville, Montréal, Québec, Canada H3C 3J7*

[b] *Materials Science Department, Coordinated Science Laboratory and the Materials Research Laboratory, University of Illinois, 1101 West Springfield Avenue, Urbana, IL 61801, USA*

Abstract

Elastic recoil detection in conjunction with time-of-flight spectroscopy (ERD–TOF) has been used to simultaneously depth profile all elements in thin SiGeC films on Si (0 0 1). Ge-rich $Si_{1-x-y}Ge_xC_y$ ($0.025 < (1-x-y) < 0.08$ and $0.026 < y < 0.216$) films were grown by ultra-high vacuum ion beam sputter deposition. X-ray diffraction and transmission electron microscopy (TEM) showed that samples with low carbon concentration (typically, $y \leq 0.07$) were single crystals with stacking faults and twins while films with $0.07 < y < 0.15$ were polycrystalline. Samples with $y > 0.15$ were amorphous. There was no evidence of SiC precipitates. Ge depth profiles were obtained from the recoil spectra as well as from the Rutherford scattered Cl spectra in the same ERD-geometry. The H concentration was determined simultaneously by selective-absorber ERD. Films with C concentrations approaching a fraction of an at.%, and Si concentrations as low as ~1 at.%, could be routinely depth profiled in a single experiment even in the presence of relatively strong surface contamination. © 1998 Elsevier Science B.V.

Keywords: $Si_{1-x-y}Ge_xC_y$; Depth profiles; Microstructures; ERD–TOF; RBS; XRD; TEM; XTEM

1. Introduction

Interest in C-based alloys of group IV elements has been growing in recent years due to their potential for band gap engineering and optoelectronic devices compatible with Si-based integrated circuit technology [1,2]. However, the equilibrium solid solubility of C in Si and Ge is extremely low (10^{17} and 10^8 cm^{-3}, respectively) [3,4]. Growth of these alloys has been reported using chemical vapour deposition (CVD), ultra high vacuum UHV (UHV–CVD) and combined ion and molecular beam deposition (CIMD) [1–14]. The key issue remains to control the incorporation on

* Corresponding author. Tel.: +1 514 343 6111 (ext. 4206); fax: +1 514 343 6215; e-mail: gujrathi@lps.umontreal.ca.

0168-583X/98/$19.00 © 1998 Elsevier Science B.V. All rights reserved.
PII S0168-583X(97)00881-1

substitutional sites. Substitutional C concentrations for molecular beam epitaxial (MBE) layers have typically been limited to ~1 at.% [5,6].

In optimizing $Si_{1-x-y}Ge_xC_y$ growth and properties, an accurate measurement of C incorporation is essential. For this application, Rutherford Back-Scattering Spectrometry (RBS) cannot be used since the C-spectrum is lost in the Ge-signal (the scattering cross-section increases with Z^2). The $^{12}C(\alpha,\alpha)^{12}C$ elastic reaction in RBS [15,16] has a resonance at 4.295 MeV which is 128 times larger than the Rutherford scattering cross-section [17] and this can be used to distinguish the C-signal from the Ge-background. However, quantification of the C concentration using the resonance technique requires a well defined (within 5 keV [15]) incident ion energy. In addition, quantitative results depend on an assumed peak shape for the resonance cross-section curve. Other practical limitations of the resonance technique are related to its relatively poor depth resolution (~100 nm in routine RBS geometry) and strong interference from surface carbon [16].

Recently, Bair et al. [18] compared C concentration measurements from (α,α) resonance with those from elastic recoil detection (ERD) with a selective absorber, using $Si_{1-x-y}Ge_xC_y$ ($0.25 < x < 0.37$ and $0.01 < y < 0.12$) samples. They concluded that ERD yielded more reliable results. However, the use of a 12 μm selective absorber to suppress forward-scattered heavy elements and probing beam ions (24 MeV Si^{5+}) deteriorated the C surface depth resolution to more than 40 nm due to energy loss straggling and multiple scattering. In addition, films thicker than ~100 nm could not be reliably studied due to overlap with the H signals. In all ion beam analysis experiments on $Si_{1-x-y}Ge_xC_y$ alloys reported in the literature, separate 2 MeV RBS measurements were required to determine the Ge and Si fractions.

In the present investigation, Ge-rich $Si_{1-x-y}Ge_xC_y$ films were deposited by UHV ion beam sputter deposition (IBSD) [19,20]. ERD in conjuction with time-of-flight (TOF) spectroscopy was used to simultaneously depth profile all elements in a single experiment. The Rutherford forward-scattered Cl spectrum was also used to provide an additional measure of the Ge concentration. Film crystallinity and microstructure, determined by transmission electron microscopy (TEM) and X-ray diffraction (XRD), were correlated with the C concentration measured by ERD.

2. Experimental procedure

All $Si_{1-x-y}Ge_xC_y$ alloys were grown in a UHV (base pressure 1×10^{-10} Torr) multi-chamber IBSD system with facilities for in situ reflection high energy electron diffraction, residual gas analysis, and Auger electron spectroscopy [19,20]. Sputtering was carried out using two independent double-grid multi-aperture broad beam ion sources with provisions for in situ spatial adjustment. The ion beam is focused by a post-extraction unipotential electrostatic ion lens which also acts as a mirror to prevent electron backscattering from the beam-neutralization device. High-purity energetic Si, Ge, and C beams were generated by bombarding the targets with 1 keV Kr^+ ions. The use of the higher-mass Kr instead of Ar together with the system geometry described in Ref. [20] dramatically decreased the flux of energetic backreflected particles. One ion gun was used to sputter a high purity Ge target while the other Kr^+ ion beam was positioned to sputter adjacent Si and C targets. The film composition was controlled through the choice of beam currents. All films were deposited at relatively low growth temperatures, $T_s = 300$–500°C, to reduce strain-induced surface roughening [21].

The substrates were $15 \times 15 \times 0.5$ mm^3 plates cleaved from p-type Si (0 0 1) wafers. Substrate cleaning consisted of degreasing [20] followed by a UV ozone treatment [22]. The wafers were then H-passivated by dipping in dilute HF [23] and immediately inserted into the vacuum system. Final substrate preparation consisted of degassing at 200°C for 30 min followed by oxide desorption at 590°C for 2 min. A 1.5 nm Ge buffer layer was grown immediately prior to $Si_{1-x-y}Ge_xC_y$ deposition.

The microstructure of the layers was determined using XRD, plan-view TEM and cross-section TEM (XTEM). The XRD measurements were performed with Mo K_α radiation using a four-axis

diffractometer capable of positioning samples to within 0.00025°. TEM and XTEM examinations were carried out using a Philips CM12 microscope operated at 120 kV. Sample preparation for TEM and XTEM consisted of mechanical grinding followed by Ar^+ ion milling [24].

Elemental depth profiles were obtained with a 30 MeV $^{35}Cl^{5+}$ beam incident at 75° from the surface normal. The detection system [25–28] is placed at an angle of −75° from the surface normal, thus recoils and ions scattered over 30° can be detected, and ingoing and outgoing paths have equal length. Two Si surface barrier detectors (SSBD), each having a 100 mm^2 circular cross-section and cooled to −10°C, were at distances of ∼65 cm from the 10 $\mu g/cm^2$ carbon foil in front of a microchannel plate (MCP) detector, resulting in 0.12 msr solid angles with the sample. The SSBD detector provides both an energy signal and a timing signal (stop) while the secondary electrons emitted by the carbon foil upon passage of an ion are detected by the MCP providing the other timing signal (start). Data were stored in an event-by-event mode and analyzed using an iterative depth profile analysis program [29]. The energy loss parameters required for the analyses were obtained from TRIM 95 which incorporates recent fine-tuning of heavy ion stopping powers [30].

The quantitative accuracy of ERD is well known [31]. The experimental setup and analysis procedure employed for the experiments described here were verified with known standards of hydrogenated Si_3N_4, SiO_2, and stoichiometric SiC. Commercial Ge doped silica glass with known Ge compositions were also used to validate the data collection and analysis. In all cases, the elemental concentrations and the film widths deduced from the depth profile plots agreed with the expected results within 2–5%.

3. Results

3.1. ERD depth profiles

An example of an ERD flight-time/energy coincidence spectrum is shown in Fig. 1 (top panel). Each coincidence event is shown as a single dot.

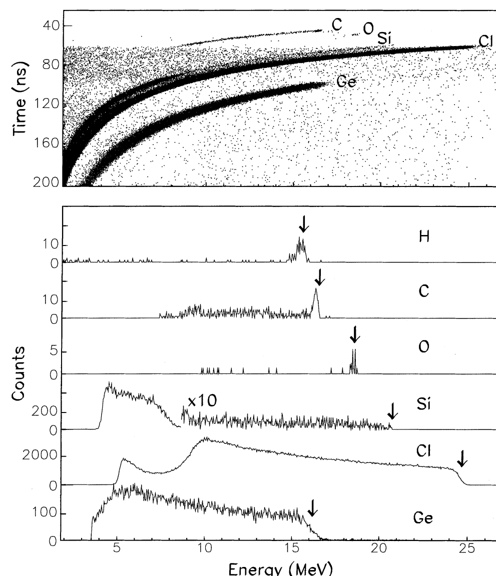

Fig. 1. (a) Flight-time vs. energy coincidence spectrum of sample 5. (b) Mass separated energy spectra obtained from data shown in (a). In addition, the H spectrum obtained from absorber ERD is shown.

Most dots fall along parabolic curves, where each curve corresponds to recoils of a certain mass. Dots that are not on such curves are mostly due to background, which determines the detection limits of impurities. The detection limit depends amongst other factors on the required depth information and in these samples amounts to approximately 0.1 at.% for C and 1.0 at.% for Si. Inspection of the curves and knowledge of the sample history shows that all target elements including surface O and C impurities due to air exposure are well resolved. Quantitative interpretation of such plots requires further analysis. All recoil events are sorted according to mass. The data can then be represented as a series of energy spectra such as those shown in Fig. 1 (bottom panels). The arrows indicate the energy of recoils originating from the free surface; counts at lower energies correspond to recoils originating from below the surface. The shape of each energy spectrum is a function of the depth distribution of each component together with its recoil cross-section and stopping power. In addition, the shape also depends on the depth distribution of the other

constituents with their respective cross-sections and stopping powers. The exception to this is the Cl spectrum, which is a standard RBS signal. In the geometry used here, only Cl scattered from Si or Ge atoms enters the detector. However, lighter species do modify the spectrum through their stopping powers.

All energy spectra were converted into depth profiles using an iterative program [29] accounting for stopping powers and recoil cross-sections. Fig. 2 shows composite depth profiles of two samples, $Si_{0.05}Ge_{0.924}C_{0.026}$ and $Si_{0.08}Ge_{0.853}C_{0.067}$. The H profile was obtained from ERD with a 4.5 mg/cm^2 Al absorber during the same experiment. Note that H and O are present only in the near-surface region. Surface C is also well resolved and distinct from the bulk C signal in the as-deposited film. While the bulk C concentration profile in the sample shown in the upper panel of Fig. 2 exhibits an increase at the film–substrate interface, the results in the lower panel establish that the C concentration is less variable in the $Si_{0.08}Ge_{0.853}C_{0.067}$ alloy. The bulk Si and Ge depth profiles remain flat throughout both samples. Table 1 summarizes the average film compositions obtained by ERD together with the XRD and TEM/XTEM microstructural information discussed in the next section.

The Ge depth profile from $Si_{0.08}Ge_{0.853}C_{0.067}$ obtained using the RBS Cl spectrum (GeRBS) is

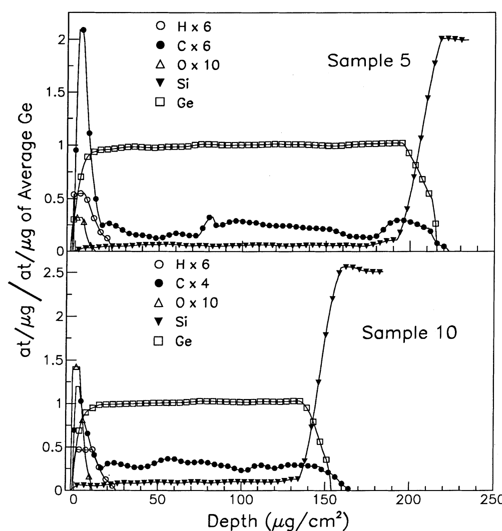

Fig. 2. Depth profiles of H, C, O, Si, and Ge of sample 5 (upper panel) and 10 (lower panel).

compared with the one deduced from the corresponding ERD spectrum (GeERD) in Fig. 3. The GeRBS profile has better depth resolution near the film–substrate interface since outgoing Cl ions suffer less energy broadening due to multiple scattering than outgoing Ge recoils. All samples exhibited very uniform GeRBS profiles while the corresponding GeERD profiles, which

Table 1
ERD and RBS compositions together with microstructural characteristics determined by TEM/XTEM and XRD. Average film densities were determined from ERD, RBS, and TEM results

Sample	T_s (°C)	Thickness (nm) ±5%	Surface roughness (nm)	C(%)	Si(%)	Si thickness (μg/cm^2)	Ge thickness (μg/cm^2)	Average film density (g/cm^3)[c]	Microstructure
5 [a]	350	430	±10	2.6	5.0	210 ± 3	212 ± 3	4.91	Polycrystal
6	500	150	±40	4.1	4.8	69 ± 1	71 ± 1	4.67	Single crystal
7	450	110 [b]		3.6	4.2	68 ± 1	68 ± 1		Single crystal
9	450	280 [b]		6.0	6.0	157 ± 2	157 ± 2		Single crystal
10	400	275	±5	6.7	8.0	149 ± 2	147 ± 2	5.38	Single crystal
14	400	300	±10	9.2	3.7	148 ± 2	146 ± 2	4.90	Polycrystal
15	400	280 [b]		12.7	6.7	145 ± 2	145 ± 2		Polycrystal
12	300	280		19.1	2.5	133 ± 2	133 ± 2		Amorphous
13	400	110	±12.5	21.6	3.0	42 ± 1	41 ± 1	3.74	Amorphous

[a] Sample grown without Ge buffer layer.
[b] Thickness estimated from the growth rates calibrated by TEM.
[c] Computed using measured Si, Ge, and C layer thickness.

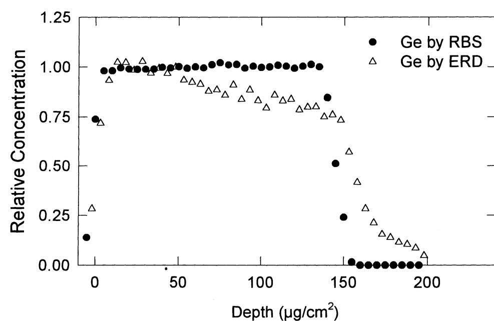

Fig. 3. Ge depth profile of sample 10 as measured by Ge ERD (open triangles) and Cl RBS (solid circles).

agreed to within 5% in the near-surface region, showed gradually decreasing apparent Ge concentrations and much deteriorated interface depth resolution. The decrease in apparent GeERD Ge concentration was about 20% at large depth (>150 μg/cm^2). This decrease, together with the apparent GeERD increase in film width compared to the corresponding GeRBS results is attributed to the larger multiple scattering effects of Ge recoils in the target as well as in the C foil (effective thickness ~20 μg/cm^2). Another source of error may be wrong stopping power data for the slow Ge recoils. The concentrations of Ge in standard samples deduced using the RBS Cl spectrum were in good agreement with known results. In addition, the thickness of deposited films, obtained from depth profiles of Si recoils was in close agreement with the results from GeRBS. Again, the Si recoils suffer less energy broadening on the way out than do the Ge recoils which comprise the GeERD spectrum. Therefore, all the Ge concentrations given in Table 1 are from GeRBS analyses.

3.2. SiGeC film microstructure

XRD, TEM, and XTEM were used to investigate the microstructure of $Si_{1-x-y}Ge_xC_y$ layers grown on a thin (~1.5 nm) Ge buffer layer on Si (0 0 1). Increasing the C fraction from $y = 0.026$ to 0.216, while keeping a low Si concentration, between 0.026 and 0.080, resulted in increased defect concentrations. Samples with $y \leq 0.07$ are single crystals whereas those with $0.07 < y < 0.15$ are polycrystalline as judged by XRD and selected-area electron diffraction (SAED) in TEM. Alloy films containing C fractions larger than 0.15 are amorphous. When grown directly on Si (0 0 1), even alloy films with C concentrations as low as 0.026 were polycrystalline due to initial reactions between C and Si as discussed below.

An XTEM bright field image, obtained using two-beam diffraction conditions with diffraction vector $g = 004$, from a 275 nm thick $Si_{0.08}Ge_{0.853}C_{0.067}$ epitaxial layer grown at $T_s = 400°C$ is shown in Fig. 4(a). The film/buffer-layer interface is smooth and abrupt with no indication of the formation of an interfacial phase. The sample surface is also relatively smooth with a roughness amplitude of ~5 nm. However, the film contains a high density of 1 1 1 stacking faults and twins. Further evidence of twinning is observed in the SAED pattern (Fig. 4(b)) – note the partial order 1/3 1 1 1 and 2/3 1 1 1 reflections – obtained from the film with the electron beam along the [1 1 0] zone axis.

An example of a polycrystalline alloy film grown on Ge/Si (0 0 1) is shown in Fig. 4(c), a bright field, $g = 220$, XTEM image from a 300 nm thick $Si_{0.037}Ge_{0.871}C_{0.092}$ alloy grown at $T_s = 400°C$. The average grain size increases from ~11 to 34 nm with increasing film thickness and the surface roughness amplitude is ~10 nm. The corresponding SAED pattern in Fig. 4(d), obtained along [1 1 0], exhibits diffraction rings composed of discrete spots.

Fig. 4(e) is a 001 bright-field plan-view TEM image from a 280 nm thick $Si_{0.067}Ge_{0.806}C_{0.127}$ sample grown at $T_s = 400°C$. The film was thinned from the backside, thus the primary contrast observed is related to surface roughness with amplitude ~10 nm. All expected diffraction rings in the SAED pattern (Fig. 4(f)) are present indicating the absence of preferred orientation in the growth direction. Small intensity modulations along the rings indicate a slight tendency toward a preferential in-plane orientation.

Elemental depth profiles from all alloy films, except sample 5 (nominally $Si_{0.05}Ge_{0.924}C_{0.026}$) were found to be quite uniform. However, the ERD profile from sample 5 exhibits a significant increase

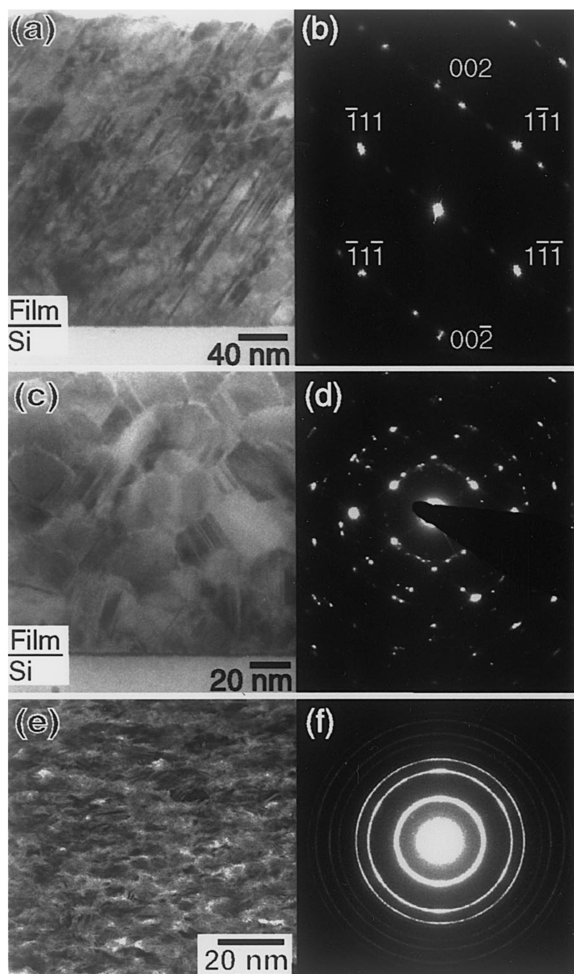

Fig. 4. (a) A bright-field ($g = 004$ near [1 1 0]) XTEM micrograph from $Si_{0.08}Ge_{0.853}C_{0.067}$ (Sample 10). (b) A [1 1 0] SAED pattern from the same sample. (c) A bright-field ($g = 220$ near [1 1 0]) XTEM micrograph from $Si_{0.037}Ge_{0.871}C_{0.092}$ (Sample 14). (d) A [1 1 0] SAED pattern from the sample shown in (c). (e) A bright-field plan-view TEM image obtained from the upper region of a nominally 200 nm thick $Si_{0.067}Ge_{0.806}C_{0.127}$ film (Sample 15). (f) SAED pattern from the sample shown in (e). The rings visible on the pattern, starting from the center are: 111, 220, 311, 422, 511, 440, 531.

in C concentration at the film/substrate interface. We believe that this excess is due to the fact that no Ge buffer layer was used in this case, leading to the formation of interfacial SiC which would also explain why this film was polycrystalline even though the bulk C concentration was low.

4. Conclusions

The elemental concentrations in Ge-rich $Si_{1-x-y}Ge_xC_y$ films grown by UHV–IBSD have been measured by ERD–TOF. Experimentally determined absolute C and Si concentrations were 2–22% and 2.5–8.0%, respectively. In contrast to α-particle backscattering resonance, data analyses did not require modelling or simulations. Surface C contamination was easily separated from bulk C due to good near-surface depth resolution, better than 10 nm. Unlike the case for (α,α) resonance detection, films thinner than 100 nm could be investigated even in the presence of strong surface contamination.

Film compositions deduced from ion flux measurements during the film growth were found to be in good agreement with the quantitative ERD results. Microstructural investigations using XTEM and XRD showed that samples with low C concentrations ($y < 0.07$) were single crystals with (1 1 1) stacking faults. Alloys with $0.07 < y < 0.15$ were polycrystalline while those with $y > 0.15$ were amorphous. No SiC precipitates were found.

In conclusion, ERD with TOF and simultaneous RBS has been demonstrated to be a very powerful technique for depth profiling all elements, including impurities, in as-deposited $Si_{1-x-y}Ge_xC_y$ films with good depth resolution.

Acknowledgements

Work at UdeM is financially supported by the Natural Sciences and Engineering Research Council of Canada (NSERC) and by the Fonds de développement des Chercheurs et de l'Aide à la Recherche (FCAR) du Québec. Research at UIUC is supported by the Office of Naval Research and the Joint Services Electronics Program. It is a pleasure to acknowledge the expert assistance of Pierre Bérichon and Réal Gosselin with the operation and maintenance of the accelerator facility.

References

[1] R.A. Soref, Proc. IEEE 81 (1993) 1687.

[2] S. Furukawa, H. Etoh, A. Ishizaka, T. Shimada, U.S. Patent #4,885,614, 5 December 1989.
[3] G. He, M.D. Savellano, H.A. Atwater, Appl. Phys. Lett. 65 (1994) 1159.
[4] R.I. Scace, G.A. Slack, J. Chem. Phys. 30 (1959) 1551.
[5] K. Eberl, S.S. Iyer, S. Zollner, J.C. Tsang, F.K. LeGoues, Appl. Phys. Lett. 60 (1992) 3033.
[6] J. Kolodzey et al., Journal of Crystal Growth 157 (1995) 386.
[7] J. Kouvetakis, M. Todd, D. Chandrasekher, D.J. Smith, Appl. Phys. Lett. 65 (1994) 2960.
[8] J.L. Regolini, F. Gisben, G. Dolino, P. Boucaud, Mater. Lett. 18 (1993) 57.
[9] N. Herbots, O.C. Hellman, U.S. Patent #4,800,100, 1989.
[10] H.J. Osten, J. Klatt, Appl. Phys. Lett. 65 (1994) 630.
[11] J. Kolodzey et al., Appl. Phys. Lett. 67 (1995) 1865.
[12] B.A. Orner et al., J. Electronic Materials 25 (1996) 297.
[13] J. Kolodzey, P.A. O'Neil, E. Hall, R. McAnnally, C.P. Swann, Inst. Phys. Conf. Ser. 137 (1993) 357.
[14] M. Todd, J. Kauvetakis David, J. Smith, Appl. Phys. Lett. 68 (1996) 2407.
[15] A.E. Bair, Z. Atzmon, S.W. Russell, T.L. Alford, J.W. Mayer, J.C. Barbour, Nucl. Instr. and Meth. B 103 (1995) 339.
[16] S. Hearne, N. Herbots, J. Xiang, P. Ye, H. Jacobsson, Nucl. Inst. and Meth. B 118 (1996) 88.
[17] J.A. Leavitt et al., Nucl. Instr. and Meth. B 40/41 (1989) 776.
[18] A.E. Bair, Z. Atzmon, S.W. Russell, J.C. Barbour, T.L. Alford, J.W. Mayer, Nucl. Inst. and Meth. B 118 (1996) 274.
[19] N.-E. Lee, M. Matsuoka, M.R. Sardela, Jr., F. Tian, J.E. Greene, J. Appl. Phys. 80 (1996) 812.
[20] G.A. Tomasch, Y.-W. Kim, L.C. Markert, N.-E. Lee, J.E. Greene, Thin Solid Films 223 (1993) 223.
[21] N.-E. Lee, D.G. Cahill, J.E. Greene, J. Appl. Phys. 80 (1997) 2199–2210.
[22] J.-P. Noël, J.E. Greene, N.L. Rowell, S. Kechang, D.C. Houghton, Appl. Phys. Lett. 55 (1989) 1525.
[23] T. Takahagi, I. Nagai, A. Ishitani, H. Kuroda, Y. Nagasawa, J. Appl. Phys. 64 (1988) 3516.
[24] J.-P. Noel et al., J. Appl. Phys. 65 (1989) 1189.
[25] R. Groleau, S.C. Gujrathi, J.-P. Martin, Nucl. Instr. and Meth. 218 (1983) 11.
[26] S.C. Gujrathi, P. Aubry, L. Lemay, J.-P. Martin, Can. J. Phys. 65 (1987) 950.
[27] S.C. Gujrathi, in: E. Sacher, J.J. Pireaux, S.P. Kowalczyk (Eds.), Metallization of Polymers, ch. 6, ACS Symp. Series No. 440, 1990, p. 88.
[28] S.C. Gujrathi, D. Poitras, J.E. Klemberg-Sapieha, L. Martinu, Nucl. Instr. and Meth. B 11 (1996) 560.
[29] K. Oxorn, S.C. Gujrathi, S. Bultena, L. Cliche, J. Miskin, Nucl. Instr. and Meth. B 45 (1990) 166.
[30] J.F. Ziegler, TRIM-95 computer code, private communication.
[31] J. Tirira, Y. Serruys, P. Trocellier, Forward Recoil Spectrometry: Applications to Hydrogen Determination in Solids, Plenum, New York, USA.